J|A|C|S
ARTICLES
Published on Web 04/11/2002

# Theoretical Evaluation of p$K_a$ in Phosphoranes: Implications for Phosphate Ester Hydrolysis

Xabier Lopez,[†,‡] Michael Schaefer,[§] Annick Dejaegere,*[,∥] and Martin Karplus*[,‡,§,⊥]

*Contribution from the Kimika Fakultatea, Euskal Herriko Unibertsitatea, P.K. 1072, 20080 Donostia, Spain, Oxford Centre for Molecular Sciences, New Chemistry Laboratory, South Parks Road, Oxford OX1 3QZ, United Kingdom, Laboratoire de Chimie Biophysique, Institut le Bel, Université Louis Pasteur, 67000 Strasbourg, France, Laboratoire de Biologie et Génomique Structurales, Ecole Supérieure de Biotechnologie de Strasbourg 67400 Illkirch, France, and Department of Chemistry and Chemical Biology, Harvard University, Cambridge, Massachusetts 02138*

Received June 4, 2001

***Abstract:*** Knowledge of the p$K_a$ of phosphoranes is important for the interpretation of phosphate ester hydrolysis. Calculated p$K_a$'s of the model phosphorane, ethylene phosphorane, are reported. The method of calculation is based on the use of dimethyl phosphate as a reference state for evaluating relative p$K_a$ values, and on the optimization of the oxygen and acidic hydrogen van der Waals radii to give reasonable p$K_a^1$, p$K_a^2$, and p$K_a^3$ for phosphoric acid in solution. Density functional theory is employed to calculate the gas-phase protonation energies, and continuum dielectric methods are used to determine the solvation corrections. The calculated p$K_a^1$ and p$K_a^2$ for the model phosphorane are 7.9 and 14.3, respectively. These values are within the range of proposed experimental values, 6.5−11.0 for p$K_a^1$, and 11.3−15.0 for p$K_a^2$. The mechanistic implications of the calculated p$K_a$'s are discussed.

## 1. Introduction

Phosphoranes are molecules with phosphorus pentacovalently bound to oxygen atoms. These compounds are important intermediates in a variety of phosphate ester hydrolysis reactions involving nucleophilic attack to form tetravalent phosphates.[1] They appear as intermediates in the hydrolysis of RNA,[2,3] as well as in phosphoryl group transfer reactions involving ATP.[4] The mechanism of these reactions is still a matter of debate,[2,3] and a knowledge of the p$K_a$'s of the phosphoranes is important for determining which of the different alternative proposals for the reaction are correct (Figure 1). Unfortunately, accurate experimental measurements for p$K_a^1$ and p$K_a^2$ for these species are not available. The proposed values range from 6.5 to 11.0 for p$K_a^1$ and from 11.3 to 15.0 for p$K_a^2$.[3] In a review on the mechanism of cleavage−transesterification of RNA[3], it was stressed that "the exact p$K_a$ value of phosphoranes should be investigated further. Knowing them will allow better interpretation of cleavage and isomerization data for phosphodiesters and RNA". Theoretical calculations can be used to supplement experimental data in cases where it is difficult to determine the p$K_a$ of certain chemical species.[5−7] In this contribution, we use density functional theory coupled with dielectric continuum methods for solvation to provide theoretical values for the p$K_a^1$ and p$K_a^2$ of ethylene phosphorane, EtP(OH)$_3$. To develop a reliable method, we use the three known p$K_a$'s of phosphoric acid to parametrize the oxygen and acidic hydrogen van der Waals parameters. The method is then applied to several isomers of EtP(OH)$_3$ and their p$K_a^1$ and p$K_a^2$ values are determined. The implications of the calculated p$K_a$'s for phosphate ester hydrolysis are discussed.

## 2. Methods

All the structures were optimized in the gas phase at B3LYP/6-31+G(d,p) level of theory using GAUSSIAN98. The B3LYP functional[9−12] was chosen because of its success in similar calculation

* Corresponding authors. E-mail addresses: (A.D.) annick@esbs.u-strasbg.fr; (M.K.) marci@tammy.harvard.edu.
† Euskal Herriko Unibertsitatea.
‡ Oxford Centre for Molecular Sciences.
§ Université Louis Pasteur.
∥ Ecole Supérieure de Biotechnologie de Strasbourg.
⊥ Harvard University.

(1) Westheimer, F. *J. Chem. Soc.* 1968, *1*, 70−78.
(2) Oivanen, M.; Kuusela, S.; Lonnberg, H. *Chem. Rev.* **1998**, *98*, 1102−1109.
(3) Perreault, D. M.; Anslyn, E. V. *Angew. Chem., Int. Ed. Engl.* **1997**, *36*, 432−450.
(4) Voet, D.; Voet, J. G.; Pratt, C. W. *Fundamentals of Biochemistry*; John Wiley and Sons: New York, 1998.
(5) Lim, C.; Bashford, D.; Karplus, M. *J. Phys. Chem.* **1991**, *95*, 5610−5620.
(6) Lyne, P.; Karplus, M. *J. Am. Chem. Soc.* 2000, *122*, 166−167.
(7) Topol, I.; Tawa, G.; Burt, S. *J. Phys. Chem. A* 1997, *101*, 10075−10081.
(8) Frisch, M. J.; Trucks, G. W.; Schlegel, H. B.; Scuseria, G. E.; Robb, M. A.; Cheeseman, J. R.; Zakrzewski, V. G.; Montgomery, J. A.; Stratmann, R. E.; Burant, J. C.; Dapprich, S.; Millam, J. M.; Daniels, A. D.; Kudin, K. N.; Strain, M. C.; O. Farkas, J. T.; Barone, V.; Cossi, M.; Cammi, R.; Mennucci, B.; Pomelli, C.; Adamo, C.; Clifford, S.; Ochterski, J.; Petersson, G. A.; Ayala, P. Y.; Cui, Q.; Morokuma, K.; Malick, D. K.; Rabuck, A. D.; Raghavachari, K.; Foresman, J. B.; Cioslowski, J.; Ortiz, J. V.; Stefanov, B. B.; Liu, G.; Liashenko, A.; Piskorz, P.; Komaromi, I.; Gomperts, R.; Martin, R. L.; Fox, D. J.; Keith, T.; Al-Laham, M. A.; Peng, C. Y.; Nanayakkara, A.; Gonzalez, C.; Challacombe, M.; Gill, P. M. W.; Johnson, B. G.; Chen, W.; Wong, M. W.; Andres, J. L.; Head-Gordon, M.; Replogle, E. S.; Pople, J. A. *Gaussian 98*, Revision A.2; Gaussian, Inc.: Pittsburgh, PA, 1998.
(9) Becke, A. *Phys. Rev. A* 1988, *38*, 3098.
(10) Lee, C.; Yang, W.; Parr, R. *Phys. Rev. B* 1988, *37*, 785.
(11) Vosko, S. H.; Wilk, L.; Nusair, M. *Can. J. Phys.* **1980**, *58*, 1200.


**10.1021/ja011373i CCC: $22.00** 

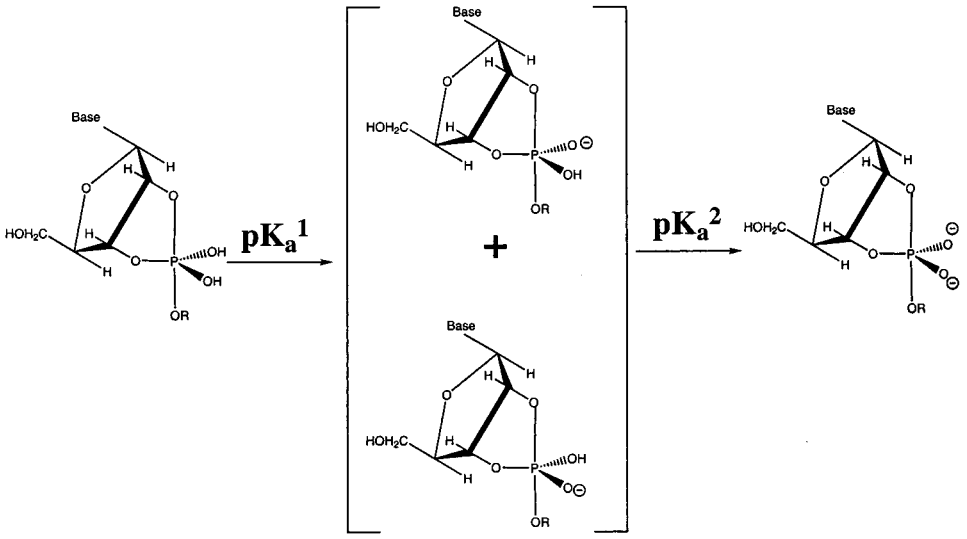


***Figure 1.*** Pentacovalent phosphorane structures found as meta-stable intermediates or transition states in the transphosphorylation and hydrolysis of RNA.

for evaluating p$K_a$ values for imidazole[7] and phosphorylated ribose.[6] To confirm that the optimized structures were minima on the potential energy surfaces, frequencies calculations were done at B3LYP/6-31+G-(d,p) level. These frequencies were then used to evaluate the zero-point vibrational energy (ZPVE) and the thermal ($T$ = 298 K) vibrational corrections to the enthalpy and Gibbs free energy[13] in the harmonic oscillator approximation. The rotational and translational energies were treated classically as $^1/_2RT$ per degrees of freedom. These calculations were also made with GAUSSIAN98.[8] To calculate the entropy, the different contributions to the partition function were evaluated using the standard expressions for an ideal gas in the canonical ensemble and the harmonic oscillator and rigid rotor approximation.

$$G = H - TS$$

$$H = E + RT$$

$$E = E_{\text{elec}} + \text{ZPVE} + E_{\text{vib}} + E_{\text{rot}} + E_{\text{trans}}$$

$E_{\text{rot}}$ and $E_{\text{trans}}$ are treated classically as $^1/_2RT$ per degrees of freedom. $E_{\text{vib}}$ is calculated in the harmonic oscillator approximation.

Solvation free energies at the gas-phase B3LYP/6-31+G(d,p) geometries were estimated with Poisson−Boltzmann calculations using the Jaguar program[14] (PB-J). In the Poisson−Boltzmann calculations performed with Jaguar, the gas-phase wave function is calculated and the electrostatic potential is determined. A set of atomic charges that fits this electrostatic potential is calculated, and these charges are passed to the Jaguar Poisson−Boltzmann solver in the program. It determines the reaction field caused by the polarization of the dielectric continuum surrounding the molecule by numerical solution of the Poisson−Boltzmann equations. This reaction field is represented as a layer of charges at the molecular surface (dielectric continuum boundary). The solvent point charges are returned to the SCF program, which performs another quantum mechanical wave function calculation, incorporating the fixed solvent charges. This process is repeated until self-consistency is obtained. The same solvation model was used in the Jaguar program for geometrical optimizations of the different species in solution. We refer to this level of theory as B3LYP(PB)/6-31+G(d,p).

## 3. Evaluation of p$K_a$ Values

**3.1. Absolute p$K_a$.** We consider phosphoric acid as a model to develop a protocol to calculate p$K_a$'s. The absolute p$K_a$ of a given acid AH is related to the standard Gibbs free energy change of the ionization reaction by the thermodynamic relationship

$$\text{p}K_a = -\log K_a = \frac{\Delta G^0_{aq}}{2.303RT} = \frac{1}{2.303RT}(G^0_{aq}(A^-) + G_{aq}(H^+) - G^0_{aq}(AH)) \quad (1)$$

where $G^0_{aq}$(X) (X = A$^-$, AH) are the free energies in solution for the protonated and unprotonated species. These are calculated from the solution-phase energies obtained from the B3LYP-(PB)/6-31+G(d,p) calculations using the Jaguar program[14] plus the zero-point vibrational energy corrections and entropic contributions calculated at the gas-phase geometries. The van der Waals radii for the nonprotonated oxygens were set to 1.42 Å on the basis of results obtained for phosphorylated ribose[6]. The gas-phase energy of the proton was determined by use of the Sackur−Tetrode equation and 1 atm for the entropic contribution (−7.76 kcal/mol) and $^5/_2RT$ was taken as the enthalpic contribution (translational energy + PV) giving a value of −6.28 kcal/mol at 298 K. The solvation free energy of the proton was set to −262.23 kcal/mol, following ref 6.

***Table 1.*** Absolute p$K_a$ Estimations for Phosphoric Acid[a]

| reaction | $Q$ | $Q + D$ | $Q + D$ (Big) | exp |
|---|---|---|---|---|
| $H_3PO_4 \leftrightarrow H_2PO_4^- + H^+$ | −2.25 | −2.25 | −2.63 | 2.30 |
| $H_2PO_4^- \leftrightarrow HPO_4^{-2} + H^+$ | 3.88 | 3.67 | 3.42 | 7.51 |
| $HPO_4^{-2} \leftrightarrow PO_4^{-3} + H^+$ | 11.48 | 11.63 | 11.60 | 11.59 |

[a] The energies in solution were evaluated using Jaguar and B3LYP/6-31+G(d,p) level of theory. Atomic charges were fit to the electrostatic potential in order to estimate the solvation free energy by solving the Poisson−Boltzmann equations, with the constraint of reproducing the total charge (first column, $Q$) or the total charge and dipole moment (second column, $Q + D$). Finally the effect of the basis set was considered by the evaluation of the energies at B3LYP/6-311++G(d,p) level of theory (third column, $Q + D$ (Big) The van der Waals radii of nonprotonated oxygens was set to 1.42 Å (Lyne et al.[6]). A temperature of 298.15 K was used for calculating the entropic contributions.

The results are given in Table 1. The experimental values of the three macroscopic p$K_a$'s of phosphoric acid are 2.12, 7.21,

(12) Becke, A. *J. Chem. Phys.* 1993, *98*, 5648.
(13) Hehre, W.; Radom, L.; Schleyer, P.; Pople, J. *Ab Initio Molecular Orbital Theory*. Wiley-Interscience, New York, 1986.
(14) Jaguar, 3.5 ed.; Schrodinger, Inc.: Portland OR, 1998.

and 12.67, which lead to microscopic p$K_a$'s of 2.30, 7.51, and 11.59 (see Appendix A). The theoretical calculations results, which are to be compared with the microscopic values, have errors for p$K_a^1$ and p$K_a^2$ of around 4 p$K_a$ units, the error for p$K_a^3$ is only of 0.11 p$K_a$ unit (11.48 versus the experimental value 11.59). We tried different constraints to determine the atomic charges for the Poisson−Boltzmann calculations. Adjusting the atomic charges to reproduce not only the total charge of the molecule but the dipole ($Q + D$ column in Table 1) did not introduce significant changes in the calculated p$K_a$'s. In addition, we evaluated the energies with a higher basis set, namely, 6-311++G(d,p) ($Q + D$ ("Big" column in Table 1) and again the calculated p$K_a$ values did not show any improvement.

**3.2. Relative p$K_a$.** As an alternative to the calculation of absolute p$K_a$'s, we evaluated relative p$K_a$'s with respect to a molecule for which the experimental p$K_a$ is known. As the reference molecule, we chose dimethyl phosphate (DMP), which has an experimental microscopic p$K_a$ of 0.99, while its macroscopic p$K_a$ is 1.29 (see Appendix A for the definition of microscopic p$K_a$). The following equilibria are considered,

$$H_3PO_4 + DMP^- \xleftrightarrow{pK^1} H_2PO_4^- + DMPH \quad (2)$$

$$H_2PO_4^- + DMP^- \xleftrightarrow{pK^2} HPO_4^{-2} + DMPH \quad (3)$$

$$HPO_4^{-2} + DMP^- \xleftrightarrow{pK^3} PO_4^{-3} + DMPH \quad (4)$$

where p$K^1$, p$K^2$ and p$K^3$ are calculated quantum mechanically; that is, to evaluate the $\Delta G_i$ corresponding to the p$K^i$, quantum calculations were performed at the B3LYP(PB)/6-31+G(d,p) level of theory using the Jaguar program[14] and the zero-point vibrational corrections and entropic contributions were calculated at the gas-phase geometries. The p$K_a$'s of phosphoric acid (i.e., p$K_a^1$, p$K_a^2$ and p$K_a^3$) are determined from the calculated $\Delta G$ values for the above equilibria and the experimental p$K_a$ of dimethyl phosphate (p$K_a^{DMPH}$(Expt)); that is,

$$pK_a^1 = pK^1 + pK_a^{DMPH}(Expt) = \frac{\Delta G_1}{\ln 10 RT} + pK_a^{DMPH}(Expt) \quad (5)$$

$$pK_a^2 = pK^2 + pK_a^{DMPH}(Expt) = \frac{\Delta G_2}{\ln 10 RT} + pK_a^{DMPH}(Expt) \quad (6)$$

$$pK_a^3 = pK^3 + pK_a^{DMPH}(Expt) = \frac{\Delta G_3}{\ln 10 RT} + pK_a^{DMPH}(Expt) \quad (7)$$

The values of the p$K_a$'s for phosphoric acid obtained in this way are listed in Table 2. The errors now are reduced to 2.01 p$K_a$ units. There are two main reasons for the improved values obtained by use of these equations for evaluating p$K_a$'s. First, a knowledge of the proton solvation energy is not required. Second, since phosphoranes and dimethyl phosphate are closely related chemical compounds, errors in evaluating the reaction free energy $\Delta G$ at a certain quantum level will cancel approximately on both sides of the eqs 5, 6 and 7. In fact, using the B3LYP(PB)/6-31+G(d,p) energies for $DMP^-$ and DMPH, we calculated an absolute p$K_a$ for DMPH of −1.06, almost 2 p$K_a$ units lower than the experimental value of 0.99; this error goes in the same direction as the error for the absolute p$K_a$ of $H_3PO_4$.

***Table 2.*** Ab Initio Reaction Energetics in Solution Evaluated with Jaguar and Using the B3LYP/6-31+G(d,p) Electron Density

| reaction | $\Delta E$ | $\Delta H$ | $T\Delta S$ | $\Delta G$ | p$K_a^{Expt}$ |
|---|---|---|---|---|---|
| $H_3PO_4 + DMP^- \leftrightarrow H_2PO_4^- + DMPH$ | −2.57 | −1.90 | −276.62 | −1.63 | |
| | (−0.90) | | | (−0.20) | (2.30) |
| $H_2PO_4^- + DMP^- \leftrightarrow HPO_4^{-2} + DMPH$ | 5.95 | 6.32 | −406.20 | 6.73 | |
| | (5.36) | | | (5.92) | (7.51) |
| $HPO_4^{-2} + DMP^- \leftrightarrow PO_4^{-3} + DMPH$ | 15.26 | 16.44 | −655.72 | 17.09 | |
| | (12.36) | | | (13.52) | (11.59) |

[a] The van der Waals radii of nonprotonated oxygens was set to 1.42 Å.[6] All quantities are in kcal/mol except for $T\Delta S$, which is in cal mol$^{-1}$. A temperature of 298 K was used. In parentheses, the p$K_a$ calculated from these reaction free energies and eqs 5, 6, and 7.

**3.3. Optimization of van der Waals Radii.** To improve the results for the p$K_a$ values, we optimized the van der Waals radii used in the Poisson−Boltzmann calculations. We defined three type of oxygens in phosphoric acid and dimethyl phosphate: unprotonated oxygen **O**, protonated oxygen (**O**H) and phosphoester oxygen (P−**O**−C) (this last type of oxygen appears only in dimethyl phosphate). In addition we also optimized the van der Waals radii of the acidic proton (**H**O). The geometries were fixed at the B3LYP(PB) structures obtained with the 1.42 Å radius for the unprotonated oxygens. We used a genetic algorithm program[15,16] to minimize the following error function,

$$\text{error} = \sum_{i=1}^{3} \frac{|pK_a^i[\text{Calc}] - pK_a^i[\text{Expt}]|}{3} \quad (8)$$

where p$K_a^i$, correspond to the first, second, and third p$K_a$'s of phosphoric acid, as calculated with eqs 5, 6, and 7 as a function of the p$K^i$ or $\Delta G^i$ obtained from eqs 2, 3, and 4.

To avoid unphysical values, we introduced limits on the range of the values for the radii. For the unprotonated oxygen, we constrained the possible values to ±0.2 Å of the 1.42 Å radius in ref 6. The protonated oxygen and phosphoester oxygen could take any value between ±0.2 Å of 1.600 Å (default radius used in Jaguar), and for the acidic hydrogen we used a ±0.150 Å limit relative to 1.150 Å (default radius of Jaguar). Preliminary calculations showed a tendency for the radius of the phosphoester oxygen to be reduced and pass the limit of 1.400 Å; therefore, we allowed a further −0.2 Å variation; that is, in the final calculation, we allowed the phosphoester oxygen to take values in the range of 1.200−1.800 Å. A population size of five chromosomes with six bits to represent each of the radii was used, and the calculations ran for 25 generations.

The results are given in Table 3. Using the default values of Jaguar for the van der Waals radii and eqs 5, 6, and 7, we obtained rather poor results with a mean error of 2.99 p$K_a$ units. Using the van der Waals radii proposed by Lyne et al.,[6] the results improved significantly, with a mean error of 2.01 (see also Table 1). However, the results were somewhat misleading, since the biggest improvement using the 1.42 Å radius for nonprotonated oxygens was for p$K_a^3$, whereas p$K_a^1$ and p$K_a^2$ showed worse agreement with experiment than with the default

(15) Carroll, D. *AIAA J.* **1996**, *34*, 338−346.
(16) Carroll, D. L. Genetic Algorithms and Optimizing Chemical Oxygen-Iodine Lasers. In *Developments in Theoretical and Applied Mechanics*; School of Engineering, The University of Alabama: Tuscaloosa, AL, 1996; Vol. XVIII.

***Table 3.*** Dependence of $pK_a$ Values on van der Waals Radii of the Nonprotonated Oxygen (O), Protonated Oxygen (OH) and Phosphoester Oxygen (OC), for the Evaluation of $pK_a$'s of Phosphoric Acid

| | atom | | | | | | | |
|---|---|---|---|---|---|---|---|---|
| | O | OH | P OC | HO | $pK_a^1$ | $pK_a^2$ | $pK_a^3$ | mean error |
| expt | | | | | 2.30 | 7.51 | 11.59 | |
| Bondi | 1.561 | 1.464 | 1.192 | 1.150 | 0.63 | 8.15 | 18.04 | 2.92 |
| Jaguar | 1.600 | 1.600 | 1.600 | 1.150 | 0.23 | 8.05 | 17.96 | 2.99 |
| Lyne | 1.420 | 1.600 | 1.600 | 1.150 | -0.20 | 5.92 | 13.52 | 2.01 |
| GA-25 | 1.444 | 1.496 | 1.169 | 1.010 | 1.02 | 6.57 | 14.17 | 1.60 |
| GA-OPT | | | | | 1.62 | 6.96 | 14.96 | 1.53 |

[a] Calculations done with eqs 5, 6, and 7. After 25 generations (GA-25) the program was stopped. GA-OPT corresponds to the same radii as GA-25 but optimizing the geometries with these radii.

Jaguar radii. Bondi radii[17] showed a slight improvement of $pK_a^1$ with respect to the Jaguar values. However, a large deviation was still observed for $pK_a^3$. Thus, optimization of the radii was necessary to obtain satisfactory results for all the $pK_a$ values of phosphoric acid.

The values of the radii obtained from the GA optimization are listed in Table 3. After 25 generations, the mean error in the $pK_a$'s of phosphoric acid is 1.60, with a significant improvement and similar deviation for $pK_a^1$ and $pK_a^2$. Using these radii, we then optimized the geometries of each species and recalculated the $pK_a$'s with the optimized geometries. The results (GA-OPT row in Table 3) showed a lower mean deviation of the $pK_a$'s (1.53 $pK_a$ units). In particular, the geometry optimization significantly improved the values of $pK_a$ and $pK_a^2$ (1.62 and 6.96, respectively) but increased the error for $pK_a^3$ (14.96). Thus, the van der Waals radii proposed here gave reasonable results for all the $pK_a$'s of phosphoric acid and very good results, within 0.6 $pK_a$ units, for $pK_a^1$ and $pK_a^2$. The latter are most important for the phosphoranes, since only singly and doubly negative charged species occur. The final van der Waals radii are rather close to those proposed by Bondi. However, the $pK_a$'s are much better, indicating the sensitivity of the latter to the former.

## 4. Application to Phosphoranes

The phosphoranes depicted in Figure 3 can be taken as a model for the phosphorane intermediates considered in mechanistic analyses of the enzymatic hydrolysis of RNA.[2,3] There are three possible protonation states: neutral/diprotic, monoanionic/monoprotic, and dianionic. For the neutral/diprotic and the monoanionic/monoprotic protonation states, there are four possible isomers, depending on the orientation of the proton at the O1P and O2P atoms (for the notation, see Figure 2). There are two orientations that are local minima for these protons: a conformation where the proton is aligned with the $P-O_{ax}(C)$ axial bond and a conformation where the proton is aligned with the $P-O_{ax}(H)$ bond. All the possible combinations are depicted in Figure 3. We use the following notation for specifying each isomer: $O_{1P}^{\uparrow}$ means that the proton at O1P is in the conformation where it is oriented toward the $O_{ax}(C)$ axial oxygen, $O_{1P}^{\downarrow}$ means that the proton is oriented toward the axial $O_{ax}(H)$; and, $O_{1P}^{0}$ means that the oxygen is unprotonated. (see Figures 2 and 3).

(17) Bondi, A. *J. Phys. Chem.* **1964**, *68*, 441.

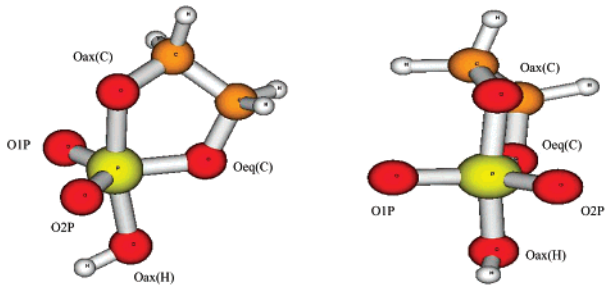


***Figure 2.*** Notation followed through the paper to refer to the two axial oxygens ($O_{ax}(C)$ and $O_{ax}(H)$) and the three equatorial oxygens (O1P, O2P, and the $O_{eq}(C)$) in the pentacovalent phosphorane structures.

***Table 4.*** B3LYP(PB)/6-31+G(d,p) Ab Initio Reaction Energetics in Solution Evaluated with Jaguar and Using the B3LYP/(PB)6-31+G(d,p) Electron Density and the Following Atomic Radii: 1.444 Å (nonprotonated oxygens), 1.496 Å (Protonated Oxygen), 1.169 (Phosphoester Oxygen, P− O−C), and 1.010 Acidic Hydrogen (H−O)[a]

| reaction | $\Delta E$ | $\Delta H$ | $T\Delta S$ | $\Delta G$ | $pK_a^{Expt}$ |
|---|---|---|---|---|---|
| $H_3PO_4 + DMP^- \leftrightarrow H_2PO_4^- + DMPH$ | −0.09 | 0.58 | −276.62 | 0.86 | |
| | (0.93) | | | (1.62) | (2.30) |
| $H_2PO_4^- + DMP^- \leftrightarrow HPO_4^{-2} + DMPH$ | 7.37 | 7.74 | −406.20 | 8.14 | |
| | (6.39) | | | (6.96) | (7.51) |
| $HPO_4^{-2} + DMP^- \leftrightarrow PO_4^{-3} + DMPH$ | 17.23 | 18.40 | −655.72 | 19.06 | |
| | (13.62) | | | (14.96) | (11.59) |

[a] All quantities are in kcal/mol except for $T\Delta S$, which is in cal $mol^{-1}$. A temperature of 298 K was used. In parentheses, the $pK_a$ calculated from these reaction energies.

***Table 5.*** Ab Initio Energies in the Gas Phase and in Solution for the Different Isomers of Phosphoranes, in Atomic Units[a]

| atom | | gas-phase | | Poisson–Boltzmann | |
|---|---|---|---|---|---|
| O1P | O2P | E | G(298) | E | G(298) |
| | | Neutral Diprotic | | | |
| ↑ | ↑ | −798.001179 | −797.921226 | −797.038753 | −797.958800 |
| | | **(2.36)** | **(2.25)** | **(0.94)** | **(0.82)** |
| ↑ | ↓ | −798.002248 | −797.922383 | −798.039231 | −797.959366 |
| | | **(1.69)** | **(1.52)** | **(0.64)** | **(0.47)** |
| ↓ | ↑ | −798.004939 | −797.924807 | −798.040246 | −797.960114 |
| | | **(0.00)** | **(0.00)** | **(0.00)** | **(0.00)** |
| ↓ | ↓ | −798.003337 | −797.922417 | −798.039550 | −797.958630 |
| | | **(1.01)** | **(1.50)** | **(0.44)** | **(0.93)** |
| | | Monoanionic/Monoprotic | | | |
| ↑ | 0 | −797.450635 | −797.38541 | −797.583603 | −797.518378 |
| | | **(0.54)** | **(0.00)** | **(0.33)** | **(0.00)** |
| 0 | ↑ | −797.451489 | −797.385289 | −797.584125 | −797.517925 |
| | | **(0.00)** | **(0.08)** | **(0.00)** | **(0.28)** |
| ↓ | 0 | −797.451163 | −797.383983 | −797.583352 | −797.516172 |
| | | **(0.20)** | **(0.90)** | **(0.49)** | **(1.38)** |
| 0 | ↓ | −797.450526 | −797.383619 | −797.583413 | −797.516506 |
| | | **(0.60)** | **(1.12)** | **(0.45)** | **(1.17)** |
| | | Dianionic | | | |
| 0 | 0 | | | −797.115222 | −797.062095 |

[a] In parentheses, the relative energies in kcal/mol with respect to the most stable isomer in each protonation state.

**4.1. Energetics and Structures.** The B3LYP/6-31g+G(d,p) absolute and relative energies and free energies in the gas phase and in solution (compared with the most stable isomer in each protonation state) are given in Table 5. The P−O bond distances are listed in Table 6 and the dipole moments in the gas-phase in Table 8. The effect of the solvent has been included through Poisson−Boltzmann calculations, using the JAGUAR program, and the optimized van der Waals radii for the different types of oxygens and the acidic proton.

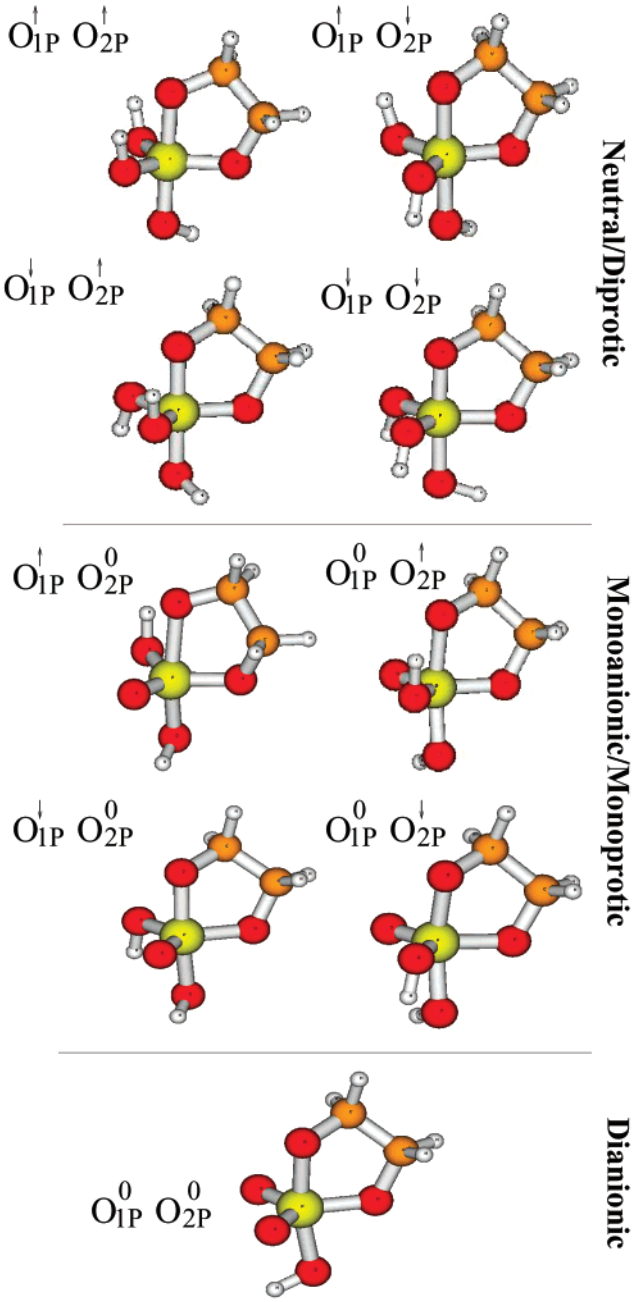


***Figure 3.*** Neutral, monoanionic, and dianionic phosphorane characterized in this work. In the case of neutral and monoanionic phosphoranes four isomers were characterized. They differ in the orientation that the protons at the phosphoryl oxygens adopt. There are two possibilities an "upward" conformation, where the proton is oriented toward the $O_{ax}(C)$ ester axial oxygen, and the "downward" conformation, in which the proton is oriented toward the $O_{ax}(H)$ axial oxygen.

**4.1.1. Neutral/Diprotic Phosphoranes.** In the gas-phase, the most stable isomer is the $O^{\downarrow}_{1P} - O^{\uparrow}_{2P}$ conformer, and the least stable is the $O^{\uparrow}_{1P} - O^{\uparrow}_{2P}$ conformer; the difference in free energy is 2.25 kcal/mol. The order of the free energies for the different isomers is:

$$O^{\downarrow}_{1P} - O^{\uparrow}_{2P}\,(0.00) < O^{\downarrow}_{1P} - O^{\downarrow}_{2P}\,(1.50) < O^{\uparrow}_{1P} - O^{\downarrow}_{2P}\,(1.52) < O^{\uparrow}_{1P} - O^{\uparrow}_{2P}\,(2.25)$$

with the numbers in parentheses in kcal/mol. These differences in free energy are attenuated by solvent, and in solution we have the following free energy differences:

$$O^{\downarrow}_{1P} - O^{\uparrow}_{2P}\,(0.00) < O^{\uparrow}_{1P} - O^{\downarrow}_{2P}\,(0.47) < O^{\uparrow}_{1P} - O^{\uparrow}_{2P}\,(0.82) < O^{\downarrow}_{1P} - O^{\downarrow}_{2P}\,(0.93)$$

The most stable isomer is still the $O^{\downarrow}_{1P} - O^{\uparrow}_{2P}$, but now the differences in free energy among the different isomers are within 1 kcal/mol. There are also some changes in the relative stabilities among the isomers; $O^{\downarrow}_{1P} - O^{\downarrow}_{2P}$ is the least stable isomer, instead of the $O^{\uparrow}_{1P} - O^{\uparrow}_{2P}$ isomer. A likely origin of the

***Table 6.*** P−O Bond Distances for the Phosphorane Structures (Å)[a]

| atom | | axial oxygens | | equatorial oxygens | | |
|---|---|---|---|---|---|---|
| O1P | O2P | P–O(C) | P–O(H) | P–O(C) | $P–O_{1P}$ | $PO_{O2P}$ |
| | | Neutral Diprotic | | | | |
| ↑ | ↑ | 1.783 | 1.645 | 1.655 | 1.636 | 1.620 |
| | | (1.735) | (1.668) | (1.654) | (1.633) | (1.622) |
| ↑ | ↓ | 1.725 | 1.679 | 1.658 | 1.637 | 1.623 |
| | | (1.729) | (1.672) | (1.652) | (1.635) | (1.621) |
| ↓ | ↑ | 1.724 | 1.677 | 1.653 | 1.627 | 1.634 |
| | | (1.720) | (1.678) | (1.649) | (1.629) | (1.629) |
| ↓ | ↓ | 1.680 | 1.726 | 1.665 | 1.631 | 1.625 |
| | | (1.711) | (1.690) | (1.653) | (1.635) | (1.621) |
| | | Monoanionic/Monoprotic | | | | |
| ↑ | 0 | 2.009 | 1.703 | 1.684 | 1.654 | 1.512 |
| | | (1.802) | (1.712) | (1.672) | (1.654) | (1.526) |
| 0 | ↑ | 1.906 | 1.711 | 1.696 | 1.519 | 1.663 |
| | | (1.790) | (1.715) | (1.674) | (1.529) | (1.648) |
| ↓ | 0 | 1.779 | 1.787 | 1.703 | 1.678 | 1.518 |
| | | (1.771) | (1.735) | (1.673) | (1.650) | (1.530) |
| 0 | ↓ | 1.783 | 1.784 | 1.705 | 1.522 | 1.669 |
| | | (1.775) | (1.734) | (1.672) | (1.530) | (1.649) |
| | | Dianionic | | | | |
| 0 | 0 | | | | | |
| | | (1.875) | (1.773) | (1.689) | (1.545) | (1.538) |

[a] The numbers without parenthesis correspond to gas-phase geometries, and the number in parentheses correspond to the geometries in solution (Poisson−Boltzmann calculations using JAGUAR). Both, gas-phase and solution-phase geometries have been obtained using the B3LYP/6-31+G(d,p) level.

***Table 7.*** Microscopic $pK_a$'s Calculated Using eq 11 and eq 12 and the Energies of Table 5[a] Macroscopic $pK_a$'s Calculated as Described in the Text

| isomer | | | | | |
|---|---|---|---|---|---|
| protonated | unprotonated | $\Delta G$ | $pK_a^{micro}$ | $pK_a^{Macro}$ | expt |
| $pK_a^1$ | | | | 7.94 | 6.5−11.0 |
| $O^{\uparrow}_{1P} - O^{\uparrow}_{2P}$ | $O^{\uparrow}_{1P} - O^{0}_{2P}$ | 8.22 | 7.02 | | |
| $O^{\uparrow}_{1P} - O^{\uparrow}_{2P}$ | $O^{0}_{1P} - O^{\uparrow}_{2P}$ | 8.50 | 7.23 | | |
| $O^{\uparrow}_{1P} - O^{\downarrow}_{2P}$ | $O^{\uparrow}_{1P} - O^{0}_{2P}$ | 8.86 | 7.49 | | |
| $O^{\uparrow}_{1P} - O^{\downarrow}_{2P}$ | $O^{0}_{1P} - O^{\downarrow}_{2P}$ | 9.75 | 8.14 | | |
| $O^{\downarrow}_{1P} - O^{\uparrow}_{2P}$ | $O^{\downarrow}_{1P} - O^{0}_{2P}$ | 10.43 | 8.64 | | |
| $O^{\downarrow}_{1P} - O^{\uparrow}_{2P}$ | $O^{0}_{1P} - O^{\uparrow}_{2P}$ | 9.33 | 7.83 | | |
| $O^{\downarrow}_{1P} - O^{\downarrow}_{2P}$ | $O^{\downarrow}_{1P} - O^{0}_{2P}$ | 9.50 | 7.95 | | |
| $O^{\downarrow}_{1P} - O^{\downarrow}_{2P}$ | $O^{0}_{1P} - O^{\downarrow}_{2P}$ | 9.29 | 7.80 | | |
| $pK_a^2$ | | | | 14.27 | 11.3−15.0 |
| $O^{\uparrow}_{1P} - O^{0}_{2P}$ | $O^{0}_{1P} - O^{0}_{2P}$ | 18.17 | 14.31 | | |
| $O^{0}_{1P} - O^{\uparrow}_{2P}$ | $O^{0}_{1P} - O^{0}_{2P}$ | 17.89 | 14.11 | | |
| $O^{\downarrow}_{1P} - O^{0}_{2P}$ | $O^{0}_{1P} - O^{0}_{2P}$ | 16.79 | 13.30 | | |
| $O^{0}_{1P} - O^{\downarrow}_{2P}$ | $O^{0}_{1P} - O^{0}_{2P}$ | 17.00 | 13.45 | | |

[a] $\Delta G$ values correspond to the $AH + DMP^- \leftrightarrow A^- + DMPH$ reaction energy in kcal/mol.

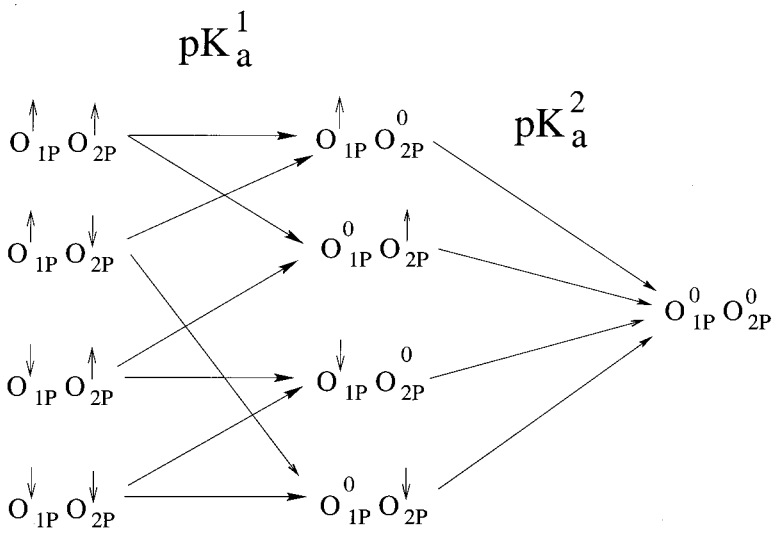


***Figure 4.*** Different possibilities for evaluating microscopic p$K_a$'s in phosphoranes. They correspond to the various combinations to remove protons from the neutral and monoanionic phosphoranes, and with the assumption that the conformation of the other phosphoryl proton is unchanged upon the ionization.

***Table 8.*** Gas-Phase Dipoles in Debye

| atom | | |
|---|---|---|
| O1P | O2P | dipole |
| | Neutral Diprotic | |
| ↑ | ↑ | 4.65 |
| ↑ | ↓ | 2.93 |
| ↓ | ↑ | 2.57 |
| ↓ | ↓ | 3.07 |
| | Monoanionic/Monoprotic | |
| ↑ | 0 | 4.16 |
| 0 | ↑ | 4.45 |
| ↓ | 0 | 4.28 |
| 0 | ↓ | 3.54 |

stabilization of $O^{\uparrow}_{1P} - O^{\uparrow}_{2P}$ is the large dipole moment for this structure, 4.654 D. (see Table 8).

The P−O bond distances obtained in the gas-phase and in solution are listed in Table 6. In general, the P−O axial bonds are longest. There are significant differences in P−O bond distances dependent on the orientation of the proton at O1P and O2P. The proton tends to elongate the P−O axial distance of the bond that is aligned with the O−H bond. Thus, for the $O^{\uparrow}_{1P} - O^{\uparrow}_{2P}$ conformer the P−$O_{ax}$(C) bond is longer, and the P−$O_{ax}$(H) bond is shorter, whereas for the $O^{\downarrow}_{1P} - O^{\downarrow}_{2P}$ conformer, the P−$O_{ax}$(C) bond is longer and the P−$O_{ax}$(H) is shorter (see Table 6). The other P−O bond distances (the equatorial bonds) show little change in the different neutral conformers.

**4.1.2. Monoanionic/Monoprotic phosphoranes.** In the gas-phase, the four isomers have very similar energies (see Figure 3); they are all within 0.6 kcal/mol. When entropic contributions are added the difference increases to 1.12 kcal/mol. The isomer with the lowest electronic energy corresponds to the $O^{0}_{1P} - O^{\uparrow}_{2P}$ isomer, but when entropic contributions are added, $O^{0}_{1P} - O^{\uparrow}_{2P}$ and $O^{\uparrow}_{1P} - O^{0}_{2P}$ have very similar energies, within 0.08 kcal/mol. For the gas-phase free energies, the order is,

$O^{\uparrow}_{1P} - O^{0}_{2P}$ (0.00) ≈ $O^{0}_{1P} - O^{\uparrow}_{2P}$ (0.08) < $O^{\downarrow}_{1P} - O^{0}_{2P}$ (0.90) < $O^{0}_{1P} - O^{\downarrow}_{2P}$ (1.12) When solvent contributions are added, the relative free energies are, $O^{\uparrow}_{1P} - O^{0}_{2P}$ (0.00) < $O^{0}_{1P} - O^{\uparrow}_{2P}$ (0.28) < $O^{0}_{1P} - O^{\downarrow}_{2P}$ (1.17) < $O^{\downarrow}_{1P} - O^{0}_{2P}$ (1.38) The solvent introduces only slight changes in the relative free energies. The most significant effect is the stabilization of the $O^{0}_{1P} - O^{\downarrow}_{2P}$ isomer with respect to $O^{\downarrow}_{1P} - O^{0}_{2P}$.

The P−O bond distances for all isomers in the gas-phase and in solution are given in Table 6. The P−O bond distances tend to be longer that in the neutral case. As for the neutral isomers, we observe that the orientation of the proton at O1P and O2P has a significant influence on the P−O axial bond distances, lengthening the P−O axial bond with respect to which the O−H bond is aligned (P−$O_{ax}$(C) in the case of ↑ conformations and P−$O_{ax}$(H) for ↓ isomers). The longest P−O axial bond is the P−$O_{ax}$(C) bond in the $O^{\uparrow}_{1P} - O^{0}_{2P}$ conformer (2.009/1.802 Å for gas-phase/solution). This could have mechanistic consequences on the reaction; i.e., since the $O^{\uparrow}_{1P} - O^{0}_{2P}$ is the longest P−$O_{ax}$(C) bond, it could be that the latter is broken preferentially in this isomer. In terms of P−O equatorial bonds, the largest differences among the isomers come from the phosphoryl oxygens being protonated (∼1.65 Å) or not (∼1.55 Å). In general, the solvent tends to shorten the long P−O axial bond distances and the equatorial phosphoester and P−O(H) bonds, whereas it elongates the equatorial P−O nonprotonated bonds. Thus, the variation in bond lengths is smaller in solution than the gas phase.

**4.1.3. Dianionic Phosphorane.** There is one dianionic phosphorane (Figure 3). In the gas phase, it is so unstable that attempts to optimize the structure led to the breaking of the P−$O_{ax}$(C) bond, yielding a phosphate product. When solvation was included, a stable dianionic phosphorane was obtained. The energies are given in Table 5 and the P−O bond distances in Table 6. It is striking that the P−O axial bond distances are the longest observed in all the phosphoranes that were studied. This confirms the trend that the larger the negative charge of the phosphorane, the longer are the P−O axial bonds.

**4.2. Estimation of p$K^1_a$ and p$K^2_a$. 4.2.1. Microscopic p$K_a$'s.** We use the protocol developed in section 3 to estimate p$K^1_a$ and p$K^2_a$ for the phosphorane intermediates. Due to the multiplicity of neutral and monoanionic states, there are eight microscopic p$K^1_a$'s and four microscopic p$K^2_a$'s, depending on which isomer is chosen for the proton abstraction (see scheme in Figure 4). Following the approach employed for phosphoric acid in section 3, we use the solution free energies given in

Table 5 and the DMPH free energies in Table 4, to evaluate the reaction free-energies ($\Delta G_1$ and $\Delta G_2$) for the following equilibria,

$$EtP(OH)_3 + DMP^- \xleftrightarrow{pK^1} EtP(OH)_2O^- + DMPH \quad (9)$$

$$EtP(OH)_2O^- + DMP^- \xleftrightarrow{pK^2} EtP(OH)O_{2-2} + DMPH \quad (10)$$

The $pK_a$'s for the phosphorane species (i.e., $pK_a^1$ and $pK_a^2$) can be determined from the calculated p$K$ or $\Delta G$ values for the above equilibria and the experimental $pK_a$ of dimethyl phosphate ($pK_a^{DMPH}$(Expt)); that is, from eqs 9 and 10 using the following formulas:

$$pK_a^1 = pK^1 + pK_a^{DMPH}(\text{Expt}) = \frac{\Delta G_1}{\ln 10 RT} + pK_a^{DMPH}(\text{Expt}) \quad (11)$$

$$pK_a^2 = pK^2 + pK_a^{DMPH}(\text{Expt}) = \frac{\Delta G_2}{\ln 10 RT} + pK_a^{DMPH}(\text{Expt}) \quad (12)$$

Microscopic $pK_a$ values were calculated for all the different possibilities in Figure 4; the results are given in Table 7. The values of $pK_a^1$(micro) range from 7.02 ($O^{\uparrow}_{1P} - O^{\uparrow}_{2P} \rightarrow O^{\uparrow}_{1P} - O^{0}_{2P}$) to 8.64 ($O^{\downarrow}_{1P} - O^{\uparrow}_{2P} \rightarrow O^{\downarrow}_{1P} - O^{0}_{2P}$). The values of $pK_a^2$(micro) are between 13.30 ($O^{\downarrow}_{1P} - O^{0}_{2P} \rightarrow O^{0}_{1P} - O^{0}_{2P}$) and 14.31 ($O^{\uparrow}_{1P} - O^{0}_{2P} \rightarrow O^{0}_{1P} - O^{0}_{2P}$). To compare with the experimental values the corresponding macroscopic $pK_a$'s have to be calculated.

**4.2.2. Macroscopic $pK_a$'s.** The macroscopic $pK_a$ can be obtained by summing over all the microscopic species, weighted according to the Boltzmann factor. The probability of finding a given isomer is given by its Boltzmann distribution

$$P(i) = \frac{e^{(-\Delta G_i/RT)}}{\sum_i e^{(-\Delta G_i/RT)}} \quad (13)$$

where $i$ runs over the different isomers for a given charge state and $\Delta G_i$ is the relative free energy of state $i$ with respect to the most stable isomer. The macroscopic free energy for each charge state $s$ (i.e., neutral, monoanionic, and dianionic) can be determined from the free energies of each microscopic state as

$$G(s) = \frac{\sum_i G_i e^{(-\Delta G_i/RT)}}{\sum_i e^{(-\Delta G_i/RT)}} \quad (14)$$

Using this formula and the $\Delta G$ and $G$ values in Table 5, we obtain a value of −797.959390 au for $G_{Neutral}$ and a value of −797.517624 au for $G_{monoanionic}$; that for the unique dianionic species is −797.062095 au. With these values we estimated the macroscopic $pK_a^1$ and $pK_a^2$ to be 7.94 and 14.27, respectively (Table 7). These values fall inside the range of experimental $pK_a$'s (6.5 to 11 for $pK_a^1$ and 11.3 to 15 for $pK_a^2$) proposed for phosphoranes.

## 5. Discussion

Pentacovalent phosphoranes have been proposed as reaction intermediates or transition states in a variety of phosphate-transfer reactions in solution and in enzymes.[1−3] The exact nature of the phosphoranes (i.e., intermediates vs transition states) as well as their protonation states remains uncertain. In the absence of direct experimental evidence, such as isolation of stable phosphoranes and experimental $pK_a$ measurements, kinetic data, and analysis of reaction products have been used to deduce the existence and protonation state of the phosphoranes involved. It has been observed in several instances that the hydrolysis reactions of phosphate esters can yield more than one reaction product. For example, methyl ethylene phosphate undergoes exocyclic as well as endocyclic cleavage during hydrolysis;[18] 3′,5′-ribonucleotides undergo cleavage but also isomerization to a 2′,5′-ribonucleotide,[2,19] and $^{18}$O-exchange between isotopically labeled water and phosphoesters is observed together with cleavage for small organic esters such as dimethyl phosphate and ethylene phosphate.[20] The interpretation of these data has generally involved the assumption that there is a pentacoordinated phosphorane intermediate, which can either cleave directly or isomerize by pseudorotation followed by cleavage (Figure 5).

The kinetics and mechanisms of phosphate transfer reactions are sensitive to external conditions, particularly to pH. For example, the hydrolysis reactions of 3′,5′-dinucleotides such as UpU, UpA, ApU, and ApA, have been studied over a pH range from −0.2 up to 12.4 (for a review see ref 2) and also in the presence of imidazolium/imidazole and related buffers.[19] In all cases, both hydrolysis of the dinucleotide and isomerization to a 2′,5′-dinucleotide are observed, but the dependence of the two reactions on pH is different. Cleavage is catalyzed by acid and base, while isomerization is acid-catalyzed below pH 4, does not depend on pH between pH 4−8, and is not observed above pH 8. The absence of isomerization reactions in basic solution is not limited to dinucleotides but has been observed for phosphodiesters and triesters,[18,20] although isomerization has been observed in very basic (pH > 14) solution for methyl ethylene phosphate[18] Two explanations have been put forward to explain that isomerization is not observed in basic solution. One is that cleavage is faster than pseudorotation at basic pH's and therefore the cleaved product is observed even though the reaction is thought to proceed through a stable monoanionic phosphorane intermediate;[18] see Figure 5. An alternative explanation is that in basic solution the reaction proceeds through a dianionic phosphorane, which is unstable, and does not have time for pseudorotation or protonation, and there is rapid cleavage to the product.[19,2]

Our calculation of the $pK_a$'s for a cyclic phosphorane gives information on the structure, energetics and protonation state of a pentacovalent phosphorane intermediate. The $pK_a$ values (cf. Table 7) correspond to standard free energies of deprotonation of 11 kcal/mol for the neutral phosphorane and 19 kcal/mol for the monoanionic phosphorane. The calculated $pK_a$'s imply that the dominant species in acidic solution is a neutral phosphorane and in the neutral range is a monoanionic species. At very low pH, a cationic species could also exist, but the

(18) Kluger, R.; Covitz, F.; Dennis, E.; Williams, L.; Westheimer, F. *J. Am. Chem. Soc.* **1969**, *91*, 6066.
(19) Breslow, R.; Dong, S. D.; Xu, R. *J. Am. Chem. Soc.* **1996**, *118*, 6588−6600.
(20) Haake, P.; Westheimer, F. *J. Am. Chem. Soc.* **1960**, *83*, 1102−1109.
(21) Jarvinen, P.; Oivanen, M.; Lonnberg, H. *J. Org. Chem.* **1991**, *56*, 5396−5401.

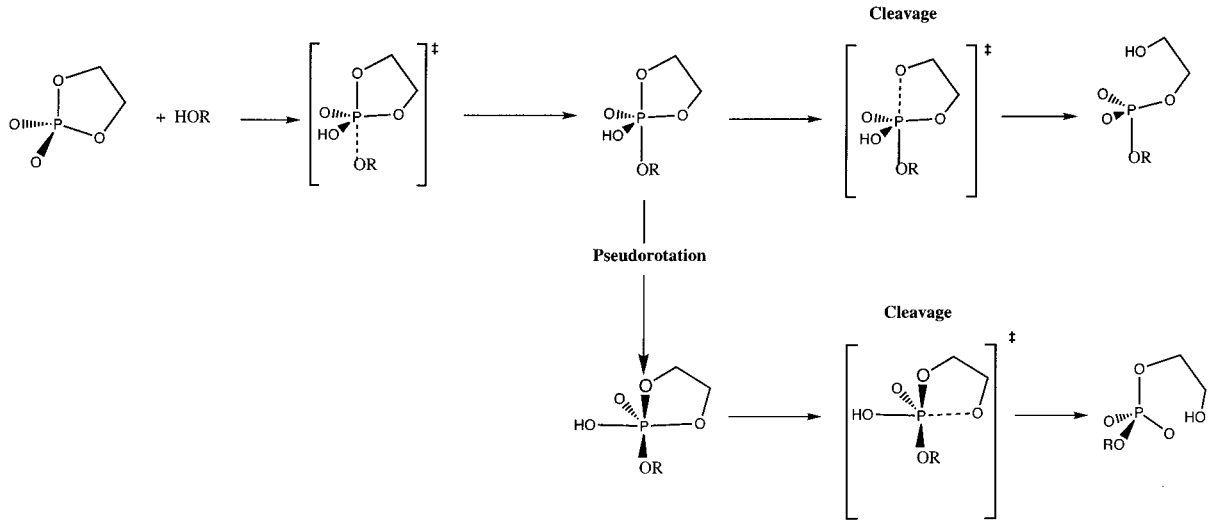


***Figure 5.*** In-line cleavage versus pseudorotation mechanisms in the hydrolysis of ethylene phosphate.

associated p$K_a$ has not been evaluated, as our main interest is in base-catalyzed hydrolysis.

Between pH 8 and 14 the calculated p$K_a$ values, which are in the experimentally estimated range, indicate that monoanionic/monoprotic species dominate and only in extremely basic solution would a dianionic phosphorane exist.

These data on phosphorane intermediates provide information on the cleavage versus isomerization process. Isomerization is thought to involve stable phosphorane intermediates. As mentioned above, cleavage of the dinucleotide UpU is catalyzed by acid between pH 3−5 and base between pH 6−11, while isomerization is acid-catalyzed below pH 4, does not depend on pH between pH 4−8, and is not observed above pH 8.[21] In the case of methyl ethylene phosphate[18] exocyclic cleavage is observed between pH 2−8 and above pH 14. As observed by Perreault and Anslyn[3], "if the p$K_a$ values of the phophoranes influence the ratio of endo to exocyclic cleavage, one would expect change in this ration at pH values near the p$K_a$ values and little change at intermediate values". Our calculated p$K_a$ values of 7.9 and 14.3 bracket the region (pH 8−14) where isomerization of methyl ethylene phosphate is not observed and are thus coherent with the above proposal.[18,3] Moreover, since the dominant species is the neutral phosphorane in the pH region (up to pH 8) where isomerization is observed, the data indicate that isomerization occurs by way of the neutral phosphorane. However for a detailed interpretation of the isomerization versus cleavage pathway, it is necessary to have information on the free energy barriers for pseudorotation versus breakdown of the phosphorane. This implies to identifiy transition states in solution for the two pathways. Calculations along this way are in progress.

## 6. Conclusions

This paper has developed a protocol for calculating the values of p$K_a^1$ and p$K_a^2$ for a model phosphorane compound based on estimates of the p$K_a$ for phosphoric acid. The protocol uses calculations of p$K_a$'s relative to dimethyl phosphate, and then optimizes the van der Waals radii of oxygens and the acidic hydrogen to give reasonable values for the known p$K_a^1$, p$K_a^2$, and p$K_a^3$ of phosphoric acid. This protocol allowed us to estimate the p$K_a$'s of a pentacovalent oxyphosphorane (Figure 2). These p$K_a$'s are important for understanding the mechanism of phosphate transfer reactions. They have been very difficult to obtain by non computational means, so that the proposed range of experimental values was large (p$K_a^1$ 6.5−11; p$K_a^2$ 11−15). The calculated values of 7.9 and 14.3 are within the experimental range. They are consistent with the observed ratio of exo- to endocyclic cleavage in methyl ethylene phosphate. They indicate that the dominant species in the acidic region up to pH 8 is the neutral phosphorane and suggest that pseudorotation proceeds through the neutral species. Further calculations are in progress to identify transition states for cleavage and pseudorotation of the phosphoranes, which will help define the reactions pathways that are possible in the various pH ranges.

**Acknowledgment.** We thank C. Maerker for helpful discussion and the suggestion of the use of reference compounds for the p$K_a$ calculations. We thank the reviewers for helpful comments. We thank the Institut de Developpement et des Ressources en Informatique Scientifique (IDRIS) for a generous allocation of CRAY computer time and the C.N.R.S. (France) for support of this work. Part of the research done at Harvard was supported by a grant from the National Institutes of Health. X.L. and M.K. thank the Oxford Molecular Centre, and especially, Professor W. Graham Richards and his group for useful discussions and access to computer facilities.

## Appendix A: Macroscopic versus Microscopic p$K_a$'s

We consider the following macroscopic equilibrium

$$AH \overset{pK_a^{Macro}}{\longleftrightarrow} A^- + H^+ \tag{15}$$

with the macroscopic p$K_a^{Macro}$ defined by

$$pK_a^{Macro} = -\log \frac{[A^-][H^+]}{[AH]} \tag{16}$$

The protonated species AH is assumed to have *n* indistinguishable microscopic states (e.g., in the case of $H_3PO_4$ there are four indistinguishable microscopic states, depending on which specific oxygen is unprotonated), and its unprotonated counterpart $A^-$ to have *m* indistinguishable states. Then the microscopic p$K_a$ corresponding to the equilibrium between

microscopic protonated and unprotonated species can be related to the macroscopic p*K*a through the formula

$$pK_a^{Macro} = -\log \frac{m[A^-]_{micro}[H^+]}{n[AH]_{micro}} \quad (17)$$

$$= pK_a^{micro} + \log \frac{n}{m} \quad (18)$$

Using phosphoric acid as an example, the three measured macroscopic p$K_a$'s of phosphoric acid are 2.12, 7.21 and 12.67. The number of undistinguishable states for each protonation state are 4 for $H_3PO_4$, 6 for $H_2PO_4^-$, 12 for $HPO_4^{-2}$ and 1 for $PO_4^{-3}$. The four undistinguishable microscopic states for $H_3PO_4$ comes from the fact that we have four oxygens that could be unprotonated. The six states for $H_2PO_4^-$ represent all the different combinations of assigning the two protons among the four oxygens. On the other hand, the 12 possibilities for $HPO_4^{-2}$ should be read as 4*3, where 4 is arising from the assignment of the proton to a given oxygen and the factor 3 arises from the fact that in each microscopic state there are three equivalent conformations of the proton. When ones consider these factors the three microscopic p$K_a$'s of phosphoric acid are 2.30, 7.51, and 11.59.

JA011373I